

Fast beam-ion instability. I. Linear theory and simulations

T. O. Raubenheimer and F. Zimmermann

Stanford Linear Accelerator Center, Stanford University, Stanford, California 94309

(Received 13 April 1995)

The interaction of an electron beam with residual gas ions results in mutually driven transverse oscillations. This effect arises during the passage of a single train of bunches. An equivalent instability mechanism is encountered in positron beams where ionization electrons oscillate within a single bunch. In either case, the oscillations grow exponentially with an exponent proportional to $t^{1/2}$. In this paper, the rise time of the instability is calculated analytically by a perturbation series approach and is compared with computer simulations. Growth rates are evaluated for several existing or proposed storage rings and linear accelerators; the effect considered could be a significant limitation in many of the future designs.

PACS number(s): 29.27.Bd, 29.17.+w, 29.20.Dh

I. INTRODUCTION

The instability mechanism described in this paper is caused by residual gas ions or electrons. Both the nature of the instability and the analytical treatment chosen resemble the beam breakup due to transverse wake fields [1,2]. The effect discussed here may occur on different time and length scales, involve different species of particles, and be a single-bunch or a multibunch effect for positron and electron beams, respectively. Charged particle beams, traversing a beam line or circulating in a storage ring, ionize the residual gas and generate free ions and electrons. The ionized atomic electrons, trapped inside a positron bunch, are strongly focused and oscillate at high frequency, thereby causing a transverse deformation of the beam. The wavelength of the oscillation is typically a small fraction of the bunch length. In much the same manner, a long train of electron bunches can interact with positive ions, resulting in a mutual excitation of the beam and the ions. Due to the mass difference of electrons and ions, the wavelength of the ion oscillation within the electron bunch train is several orders of magnitude larger than that of the electrons within a single positron bunch.

The effect described arises during the passage of a single electron-bunch train or a single positron bunch; ions (or ionized electrons) created by the head of the train (bunch) perturb the tail. The instability mechanism is the same in linear accelerators and storage rings where we assume that the ions are not trapped from turn to turn. It differs from instabilities previously studied [2–8], where the ions, usually treated as being in equilibrium, interact with a circulating electron or antiproton beam. The two-beam instability theory developed by Koshkarev and Zenkevich [9] and Laslett *et al.* [10] explains the dependence of the beam-ion interaction upon the ion oscillation frequency and the betatron tunes of the storage ring. However, it does not describe the instability we discuss that can occur in a transport line, linear accelerator, or a storage ring with a clearing gap to prevent ion trapping.

This paper is structured as follows. In Sec. II the dif-

ferential equations of motion are given. Section III discusses the underlying assumptions and approximations. For a rectangular beam distribution, the equations of motion are solved by a perturbation expansion in Sec. IV, where expressions for the instability rise time are derived. Section V describes the computer simulations performed for several accelerators and compares the simulation data with the analytical results. In Sec. VI rise times are evaluated for several operating or proposed storage rings and linear accelerators. Section VII is devoted to a brief discussion of possible remedies. Results are summarized and a perspective on open questions is given in Section VIII.

II. EQUATIONS OF MOTION

The vertical motion of the beam and the ions or electrons generated during the beam passage via ionization of the residual gas is a mutually driven oscillation, which, in linear approximation, may be described by two equations of motion. The first equation reads

$$\frac{d^2 y_b(s, z)}{ds^2} + \omega_\beta^2 y_b(s, z) = K [y_i(s, s+z) - y_b(s, z)] \int_{-\infty}^z \rho(z') dz'. \quad (1)$$

The coordinate s denotes the longitudinal position along the beam line or storage ring. Equation (1) represents the vertical motion of the beam centroid $y_b(s, z)$ at a distance z from the bunch or bunch-train center. In our convention, positive values of z refer to trailing particles. The motion is a combination of a betatron oscillation due to external focusing, represented by a harmonic oscillator of frequency $\omega_\beta \approx 1/\beta_y$ and a driving force that is proportional to the distance between the beam and the ion centroids and to the number of generated ions. Thus, assuming collisional ionization, the driving force

is proportional to an integral over the beam density ρ normalized such that $\int_{-\infty}^{\infty} \rho(z) dz = 1$. Here and in the following the term "ions" shall be understood as "ions or electrons" and the term "bunch train" will refer to the "bunch train or single bunch," depending on whether we are discussing an electron bunch train or a single positron bunch.

The coefficient K is given by

$$K \equiv \frac{2\lambda_{\text{ion}}(p_{\text{gas}}) r_e}{\gamma \Sigma_y (\Sigma_y + \Sigma_x)} \approx \frac{4\lambda_{\text{ion}}(p_{\text{gas}}) r_e}{\gamma 3\sigma_y (\sigma_x + \sigma_y)}, \quad (2)$$

where γ denotes the relativistic factor $\gamma = E/(mc^2)$ for the beam, r_e is the classical electron radius, and

$$\Sigma_{x,y}^2 = \sigma_{x,y}^2 + \sigma_{\text{ion},x,y}^2 \approx \frac{3}{2} \sigma_{x,y}^2. \quad (3)$$

The term $\sigma_{x,y}$ denotes the horizontal and the vertical rms beam size, respectively. Assuming that the ions are generated at rest (i.e., at temperature zero), the average rms size of the ion cloud is smaller by a factor $\sqrt{2}$ due to focusing by the beam. The ions also have a non-Gaussian transverse distribution, but the force on the beam closely approximates that of a Gaussian bunch. Assuming a cross section for collisional ionization of about 2 Mb (corresponding to carbon monoxide at 40 GeV) the density λ_{ion} of ions per meter at the end of the bunch train is

$$\lambda_{\text{ion}} \text{ (m}^{-1}\text{)} \approx 6N p_{\text{gas}} \text{ (Torr)}, \quad (4)$$

where N is the total number of particles in the beam, p_{gas} is the residual gas pressure in torr, and other quantities are in SI units, which are used throughout the paper. The number of ions per meter generated by the beam per unit time at a distance z from the bunch center is

$$\dot{\lambda}_{\text{ion}} \text{ (m}^{-1} \text{ s}^{-1}\text{)} = c\rho(z)\lambda_{\text{ion}} \approx 1.8 \times 10^9 \rho(z) \text{ (m}^{-1}\text{)} p_{\text{gas}} \text{ (Torr)}, \quad (5)$$

where c denotes the velocity of light.

The second equation

$$\frac{d^2 \tilde{y}_i(s,t)}{dt^2} + \omega_i^2(ct-s) \tilde{y}_i(s,t) = \omega_i^2(z) y_b(s, ct-s) \quad (6)$$

with the appropriate initial conditions describes a transverse slice of ions or electrons, at fixed position s , oscillating in time inside the beam. The variable $\tilde{y}_i(s,t)$ is the vertical centroid of the transverse slice of ions. At a certain time t , beam particles at a distance $z = ct - s$ from the bunch center reach the location s . Their centroid position is therefore given by $y_b(s, ct - s)$. The oscillation frequency $\omega_i(ct - s) = \omega_i(z)$ is proportional to the square root of the beam density ρ . In the case of electrons oscillating inside a single positron bunch, ω_i is given by

$$\omega_i \equiv \left[\frac{4N\rho(z)r_e}{3\sigma_y(\sigma_x + \sigma_y)} \right]^{1/2} c \quad \text{(electrons, single bunch)}, \quad (7)$$

while for ions and an electron bunch train we have

$$\omega_i \equiv \left[\frac{4N_b r_p}{3L_{\text{sep}} \sigma_y (\sigma_x + \sigma_y) A} \right]^{1/2} c \quad \text{(ions, bunch train)}, \quad (8)$$

where A designates the atomic mass number of the ions, N_b the number of particles per bunch, L_{sep} the bunch spacing, and r_p the classical proton radius ($r_p \approx 1.5 \times 10^{-18}$ m).

The solution to Eq. (5) for a slice of ions generated at time $t' = (s + z')/c$ is denoted $\tilde{y}_i(s, t|s + z')$. The centroid of the ions $y_i(s, t)$ of Eq. (1) is obtained by averaging $\tilde{y}_i(s, s + z')$ over all possible creation times, namely,

$$y_i(s, t) = \frac{\int_{-\infty}^z dz' \rho(z') \tilde{y}_i(s, t|s + z')}{\int_{-\infty}^z \rho(z') dz'}. \quad (9)$$

III. APPROXIMATIONS IN THE ANALYTICAL TREATMENT

Equations (1)–(5) involve several assumptions and approximations. The following are noteworthy.

(i) The force between beam and ions is assumed to be linear. Should the coherent oscillation grow larger than the beam size, this approximation would no longer be valid and the decay of the force at large distances would have to be considered. Furthermore, we neglect the Landau damping due to the nonlinearity of the beam-ion force. This may reduce the instability growth rate.

(ii) We ignore any Landau damping caused by the lattice, such as that due to nonlinear fields or chromaticity, which could counteract a further growth of the oscillation amplitude and give rise to filamentation.

(iii) The ion frequency is treated as constant along the beam line. This is a good approximation for a FODO lattice, but it may overestimate the effect of the ions in other cases.

(iv) It is supposed that inside a bunch train the ions are not overfocused, so that a smooth approximation of the motion in the form of Eq. (5) may be made. This condition is written

$$\frac{\omega_i L_{\text{sep}}}{c} < 2, \quad (10)$$

where L_{sep} is the distance between two bunches. Ions are, however, strongly overfocused between two different bunch trains, so we ignore the coupling between trains.

(v) The number of neutral gas molecules is assumed to be large compared with the number of ions during the full passage time of the bunch train or bunch. If there is no repopulation, this condition may also be written

$$\frac{N}{\sigma_x \sigma_y} < 3 \times 10^{22} \text{ m}^{-2}, \quad (11)$$

where N denotes the total number of electrons in the train. This condition is barely fulfilled for the main lin-

ear accelerator in the NLC [12], a future linear collider being designed at the Stanford Linear Accelerator Center (SLAC). However, saturation effects are not important when the beam area is repopulated by thermally moving gas molecules, as is usually the case. The second ionization (the cross section of which is, in general, comparable to that of the first ionization) may be important in some situations, but is not included in the present treatment.

(vi) In the case of storage rings, ions are generated not only by collisional ionization from the beam, but also by synchrotron radiation. The photoelectric cross section for photon energies below 100 eV is about 5–10 Mb, which is 3–5 times larger than the collisional ionization cross section. In total, for the SLAC PEP-II High Energy Ring (PEP-II HER) [11], the NLC Damping Ring (NLC DR) [12], and the Stanford Linear Collider (SLC) Arcs [13], there are about 2–3 times more ions generated by synchrotron radiation than by the beam electrons. Most of the former are far outside the beam area and are equally distributed between the beam and the chamber wall. Because the density of the radiation-generated ions is low compared with the density of ions generated by collisional ionization, in a first approximation, they can be ignored; the ions form a diffuse halo around the beam without affecting the dynamics, since the resulting field gradient is quite small.

(vii) The neutralization of ions by photoelectrons from the vacuum chamber walls is ignored. The probability

of this process is extremely small. Furthermore, only the small fraction of photoelectrons of sufficiently high energy may reach the beam orbit in the time interval between two bunch passages. For instance, if the bunch gap is 1.4 ns, the minimum electron energy is of the order of 3 keV.

IV. PERTURBATION EXPANSION AND RISE TIMES

In the following we make the further approximation that the longitudinal bunch density $\rho(z)$ is a rectangular distribution, namely,

$$\rho(z) = \begin{cases} \frac{1}{2z_0} & \text{for } |z| < z_0 \\ 0 & \text{otherwise} \end{cases} \quad (12)$$

In this case, the oscillation frequency ω_i is constant inside the bunch or along the bunch train. This assumption considerably simplifies the following calculations.

Consider a transverse slice of ions at position s in the accelerator created by ionization at time t' . Because the initial position of the ions must be the same as the beam that created them, the initial conditions are $\tilde{y}_i(s, t'|t') = y_b(s, ct' - s)$ and $d\tilde{y}_i(s, t'|t')/dt = 0$. From Eq. (5), the vertical position at a later time t is

$$\tilde{y}_i(s, t|t') = y_b(s, ct' - s) \cos[\omega_i(t - t')] + \omega_i \int_{t'}^t y_b(s, ct'' - s) \sin[\omega_i(t - t'')] dt'' \quad (13)$$

$$= y_b(s, ct - s) - \int_{t'}^t \frac{\partial y_b(s, ct'' - s)}{\partial t''} \cos[\omega_i(t - t'')] dt'', \quad (14)$$

where we have performed an integration by parts. The centroid of the ions or electrons is obtained from Eq. (8)

$$y_i(s, t) = y_b(s, ct - s) - \frac{1}{\int_{-z_0}^z dz' \rho(z')} \int_{-z_0}^z dz' \rho(z') \int_{z'+s}^{z+s} \frac{\partial y_b(s, ct'' - s)}{\partial t''} \cos[\omega_i(t - t'')] dt'' \quad (15)$$

or

$$y_i(s, s + z) = y_b(s, z) - \frac{1}{\int_{-z_0}^z dz' \rho(z')} \int_{-z_0}^z dz' \rho(z') \int_{z'}^z dz'' \frac{\partial y_b(s, z'')}{\partial z''} \cos[\omega_i(z - z'')] dz'', \quad (16)$$

where in the second step we have changed the variable of integration from t to $z \equiv ct - s$. According to Eq. (15), a nonzero slope $\partial y_b(s, z)/\partial z$ (i.e., a transverse displacement of at least one “slice” in z with respect to the rest of the beam) is required in order that the instability can develop. We are now in a position to combine Eqs. (1) and (5) into an integral equation for the beam centroids $y_b(s, z)$ alone. From Eq. (1) we find

$$y_b(s, z) = y_b(0, z) \cos(\omega_\beta s + \phi_0) + \frac{1}{\omega_\beta} \int_0^s ds' K \int_{-z_0}^z \rho(z') dz' [y_i(s', z + s') - y_b(s', z)] \sin[\omega_\beta(s - s')] \quad (17)$$

$$= y_b(0, z) \cos(\omega_\beta s + \phi_0) - \frac{1}{\omega_\beta} \int_0^s ds' K \sin[\omega_\beta(s - s')] \int_{-z_0}^z dz' \rho(z') \int_{z'}^z dz'' \frac{\partial y_b(s', z'')}{\partial z''} \cos[\omega_i(z - z'')] , \quad (18)$$

where the first term represents an unperturbed betatron oscillation. This integral equation may be solved by a perturbation series in K/ω_β . For that purpose we write

$$y_b(s, z) = \sum_{n=0}^{\infty} y_b^n(s, z) \tag{19}$$

and the n th-order solution $y_b^n(s, z)$ is given by the recursion relation

$$\begin{aligned} y_b^{n+1}(s, z) = & -\frac{K}{\omega_\beta} \int_{-z_0}^z dz' \rho(z') \\ & \times \int_{z'}^z dz'' \cos[\omega_i(z - z'')] \\ & \times \int_0^s ds' \sin[\omega_\beta(s - s')] \frac{\partial y_b^n(s', z'')}{\partial z''} . \end{aligned} \tag{20}$$

For the zeroth-order term $y_b^0(s, z)$ we now make the following ansatz:

$$y_b^0(s, z) = \hat{y} \cos(\omega_\beta s + \phi) \sin(\omega_i z + \theta), \tag{21}$$

where \hat{y} is the initial Fourier component of frequency ω_i in the longitudinal beam distribution. This initial amplitude could, for instance, be due to Schottky noise (i.e., the finite number of particles in which case $\hat{y} \sim 3\sigma_y/\sqrt{N}$) or vertical dispersion, etc. The s -dependent term of Eq. (21) describes a pure betatron oscillation, while the z -dependent part reflects the oscillation of the ions at a frequency ω_i for each position s ; this translates into a longitudinal deformation of the beam. The terms ϕ and θ denote initial phases. In order to solve the perturbation equation (21) it is convenient to make the further simplifying assumptions,

$$\omega_\beta s \gg 1, \tag{22}$$

$$\omega_i z_0 \gg 1. \tag{23}$$

In other words, we consider, first, the beam evolution

over time periods larger than the betatron oscillation period and, second, bunches or bunch trains that are long compared with the oscillation wavelength of the trapped particles. Both conditions are easily fulfilled for the applications considered in the later sections.

Using Eqs. (21) and (20) the first-order solution reads

$$\begin{aligned} y_b^1(s, z) = & -\frac{K\omega_i}{\omega_\beta} \left[\int_{-z_0}^z dz' \frac{1}{2z_0} \right. \\ & \times \left. \int_{z'}^z dz'' \cos[\omega_i(z - z'')] \cos(\omega_i z'' + \theta) \right] \\ & \times \left[\int_0^s ds' \sin[\omega_\beta(s - s')] \cos(\omega_\beta s' + \phi) \right] , \\ = & -\hat{y} \frac{K\omega_i}{2z_0 \omega_\beta} \left[\frac{1}{4} (z + z_0)^2 \cos(\omega_i z + \theta) \right] \\ & \times \left[\frac{s}{2} \sin(\omega_\beta s + \phi) \right] . \end{aligned} \tag{24}$$

More generally, the n th-order term in the expansion (19) is given by

$$y_b^n(s, z) = \hat{y} \left(\frac{-K}{\omega_\beta} \right)^n S_n(s) Z_n(z), \tag{25}$$

where

$$\begin{aligned} S_n(s) \equiv & \int_0^s ds^{(1)} \sin \omega_\beta(s - s^{(1)}) \dots \\ & \times \int_0^{s^{(n-1)}} ds^{(n)} \sin \omega_\beta(s^{(n-1)} - s^{(n)}) \\ & \times \cos(\omega_\beta s^{(n)} + \phi) \\ \approx & \frac{1}{n!} \frac{s^n}{2^n} \operatorname{Re} [i^n \exp\{i(\omega_\beta s + \phi)\}] \end{aligned} \tag{26}$$

and

$$\begin{aligned} Z_n(z) \equiv & \int_{-z_0}^z dz^{(1)'} \frac{1}{2z_0} \int_{z^{(1)'}}^z dz^{(1)} f(z, z^{(1)}) \dots \int_{-z_0}^{z^{(n-1)'}} dz^{(n)'} \frac{1}{2z_0} \int_{z^{(n)'}}^{z^{(n-1)'}} dz^{(n)} f(z^{(n-1)}, z^{(n)}) \sin(\omega_i z^{(n)} + \theta) \\ \approx & \left[\frac{\omega_i(z + z_0)^2}{8z_0} \right]^n \frac{1}{n!} \operatorname{Im} [i^n \exp\{i(\omega_i z + \theta)\}] , \end{aligned} \tag{27}$$

where

$$f(z, z^{(1)}) = \cos \left[\omega_i(z - z^{(1)}) \right] \frac{\partial}{\partial z^{(1)}}. \tag{28}$$

The approximate expressions for S_n and Z_n were found, assuming that the growth is small over an oscillation ω_β or ω_i . Strictly, this imposes an upper limit on s and z , but these limits are outside the regions of physical interest.

If we introduce the dimensionless function

$$\eta(s, z) \equiv \left[\frac{K\omega_i(z + z_0)^2 s}{\omega_\beta 16z_0} \right], \tag{29}$$

the solution (25) may be rewritten

$$y_b(s, z) = \frac{\hat{y}}{2} \sum_{n=0}^{\infty} \frac{\eta(s, z)^n}{(n!)^2} \times [(-1)^n \sin(\omega_i z + \theta + \omega_\beta s + \phi) + \sin(\omega_i z + \theta - \omega_\beta s - \phi)] . \quad (30)$$

Since the series expansion of the zeroth-order Bessel function J_0 is

$$J_0(z) = 1 - \frac{z^2/4}{(1!)^2} + \frac{(z^2/4)^2}{(2!)^2} - \frac{(z^2/4)^3}{(3!)^2} + \dots , \quad (31)$$

Eq. (30) can be written in a more compact form as

$$y_b(s, z) = \hat{y} \frac{1}{2} \left\{ J_0 \left[2\sqrt{\eta(s, z)} \right] \sin(\omega_i z + \omega_\beta s + \phi + \theta) + J_0 \left[2i\sqrt{\eta(s, z)} \right] \sin(\omega_i z - \omega_\beta s - \phi + \theta) \right\} . \quad (32)$$

Now the asymptotic form of the Bessel function for large arguments

$$2\sqrt{\eta(s, z)} \gg 1 \quad (33)$$

is

$$J_0(2\sqrt{\eta}) \approx \pi^{-1/2} \eta^{-1/4} \cos\left(2\sqrt{\eta} - \frac{\pi}{4}\right) , \quad (34)$$

$$J_0(2i\sqrt{\eta}) \approx (4\pi\sqrt{\eta})^{-1/2} \exp(2\sqrt{\eta}) . \quad (35)$$

In this large time limit, we find

$$y_b(s, z) \approx \hat{y} \frac{1}{4\sqrt{\pi}} \frac{1}{\eta^{1/4}} \exp(2\sqrt{\eta}) \times \sin(\omega_i z - \omega_\beta s + \theta - \phi) . \quad (36)$$

Only the term with phase $(\omega_i z - \omega_\beta s)$ is exponentially growing, while the other, of phase $(\omega_i z + \omega_\beta s)$, is damped. In the first case, the two slopes $\partial y_b / \partial s$ and $\partial y_b / \partial(-z)$ have equal sign. For a train of electron bunches, the dimensionless function $\eta(s, z)$, Eq. (29), is

$$\eta(s, z) = \frac{N_b^{3/2} r_e r_p^{1/2} (z + z_0)^3 s}{\sqrt{2} \gamma \sigma_y^{3/2} (\sigma_x + \sigma_y)^{3/2} \omega_\beta z_0 A^{1/2} L_{\text{sep}}^{3/2} p} \quad (\text{Torr}) , \quad (37)$$

where N_b denotes the number of particles per bunch, L_{sep} is the bunch spacing, $\sigma_{x,y}$ is the horizontal and the vertical beam size, A is the atomic mass number of the ions, $\gamma = E_e / (m_e c^2)$ is the relativistic factor of the beam elec-

trons, ω_β ($\approx 1/\beta_y$) is the vertical betatron frequency, r_e and r_p are the classical electron and proton radii, and all quantities are in SI units. Finally, notice that the function $\eta(s, z)$ increases linearly with time t (or with distance s) and with vacuum pressure p_{gas} and is inversely proportional to the beam energy. It scales as the 3/2 power of the number of particles per bunch and as the square of the bunch train length.

Defining a growth rate τ_{asym}^{-1} for the asymptotic limit as the time at which the exponent in Eq. (36) is equal to one, we find

$$\tau_{\text{asym}}^{-1} (\text{m}^{-1}) \equiv \frac{K \omega_i (z + z_0)^2}{4 \omega_\beta z_0} \quad (\text{asymptotic limit}) . \quad (38)$$

Note that τ_{asym} is not an e -folding time, but that asymptotically the oscillation grows as $\exp\left[\sqrt{s/(c\tau_{\text{asym}})}\right]$. For comparison, from the first-order solution Eq. (24) the small-amplitude growth rate is estimated to be

$$\tau_1^{-1} (\text{m}^{-1}) = \frac{K \omega_i (z + z_0)^2}{16 \omega_\beta z_0} \quad (\text{first-order solution}) , \quad (39)$$

which is smaller by a factor 4. For the multibunch case, the asymptotic growth rate Eq. (38) at $z = z_0$ can be expressed in terms of more basic parameters as

$$\tau_{\text{asym}, e^-}^{-1} (\text{s}^{-1}) \approx 5p (\text{Torr}) \frac{N_b^{3/2} n_b^2 r_e r_p^{1/2} L_{\text{sep}}^{1/2} c}{\gamma \sigma_y^{3/2} (\sigma_x + \sigma_y)^{3/2} A^{1/2} \omega_\beta} , \quad (40)$$

where n_b is the number of bunches and c is the velocity of light. The growth rate strongly depends on the number of bunches, the number of particles per bunch, and the beam size. In the case of a single positron bunch interacting with the atomic electrons, the asymptotic growth rate at $z = z_0$ can also be written

$$\tau_{\text{asym}, e^+}^{-1} (\text{s}^{-1}) \approx 7p (\text{Torr}) \frac{N_b^{3/2} r_e^{3/2} \sigma_z^{1/2} c}{\gamma \sigma_y^{3/2} (\sigma_x + \sigma_y)^{3/2} \omega_\beta} , \quad (41)$$

where σ_z is the rms bunch length.

Finally, the asymptotic form of the ion oscillation is obtained by inserting the asymptotic beam oscillation Eq. (36) into Eq. (16). Retaining only the largest terms, we find

$$y_i(s, s+z) \approx y_b(s, z) + \frac{\hat{y} \omega_i (z + z_0)}{8\sqrt{\eta}} [i J_1(2i\sqrt{\eta}) \cos(\omega_i z - \omega_\beta s + \theta - \phi) - J_1(2\sqrt{\eta}) \cos(\omega_i + \omega_\beta s + \theta + \phi)] \quad (42)$$

$$\approx y_b(s, z) - \frac{\hat{y} \omega_i (z + z_0)}{8\sqrt{\pi} \eta^{3/4}} \left[\frac{1}{2} \exp\{2\sqrt{\eta}\} \cos(\omega_i z - \omega_\beta s + \theta - \phi) + \sin\left(2\sqrt{\eta} - \frac{\pi}{4}\right) \cos(\omega_i z + \omega_\beta s + \theta + \phi) \right] , \quad (43)$$

$$\approx \frac{\hat{y}}{4\sqrt{\pi} \eta^{1/4}} \exp\{2\sqrt{\eta}\} \left[\sin(\omega_i z - \omega_\beta s + \theta - \phi) - \frac{\omega_i(z + z_0)}{4\eta^{1/2}} \cos(\omega_i z - \omega_\beta s + \theta - \phi) \right]. \quad (44)$$

The difference between the ion and beam amplitudes is proportional to the factor $\omega_i(z + z_0)/(4\sqrt{\eta})$ and disappears in the limit $\eta \rightarrow \infty$, for which $y_i(s, s + z) \approx y_b(s, z)$. The same is true for the phase shift between the two oscillations Eqs. (36) and (43). The linear approximation of the coupling force between the beam and the ions in Eq. (1) is no longer valid when the separation of the two centroids becomes of the order of the beam size σ_y . Since the ions and bunches oscillate with similar amplitudes, the linear approximation breaks down at about

$$y_b(s, z) \approx \sigma_y. \quad (45)$$

V. COMPUTER SIMULATIONS

To study this instability, we have written a computer simulation. The simulation treats the beam, the ions, and the ionized electrons as collections of macroparticles whose distributions are allowed to evolve self-consistently. Specifically, each bunch in the beam is divided into slices in z . Each slice is then represented by macroparticles with coordinates in $(x, x_p, y, y_p, \delta E/E)$. The number of particles per slice is chosen to reflect a Gaussian distribution between $\pm 3\sigma_z$ and the initial particle coordinates are random with Gaussian distributions. Typically, when studying the effect of trapped ions generated by an electron bunch train, each bunch is divided into five slices, while the bunch is divided into as many as 300 slices when studying the effect of the trapped electrons within a positron bunch. Finally, it is important to note that the longitudinal position z of the particles is fixed; the code was written to study linear accelerators and does not include synchrotron motion.

The slices of macroparticles are tracked through a magnet lattice. To date, we have only considered FODO lattices with or without acceleration sections between the quadrupoles. When tracking storage rings, horizontal dispersion is included and sextupole magnets can be included. The generation and motion of ions and ionized electrons and their effects on the beam are calculated at four locations in each FODO cell: at the center of each quadrupole and at the center of each drift or acceleration section.

At each lattice point, the calculations are performed using a grid in x and y centered at the bunch train centroid and extending between $\pm 5\sigma_{x,y}$. As each beam slice passes, macroparticles are created at the grid points representing the ions and ionized electrons generated by collisional and tunneling ionization. The charge density of each ion or electron macroparticle is determined by the ionization cross sections, the beam charge in the slice, and the local gas density. The local gas is depleted by the ionization process, but can partially repopulate between bunches since it is assumed to be at 300 K. The ion

and ionized electron macroparticles are created with zero initial velocity. After creation, each macroparticle is free to move in transverse phase space; longitudinal motion is ignored. The number of ion or electron macroparticles accumulates with the passage of each beam slice until the end of the bunch train. At this point, they are discarded and the calculation proceeds to the next lattice point.

As each beam slice passes, the beam fields are calculated, using the rms width of the beam macroparticle distribution and the Bassetti-Erskine formula [14], and are mapped onto the grid. The charge density of the ion and atomic electron macroparticles is also mapped onto the grid and the corresponding electric field is calculated at the grid points using the two-dimensional Coulomb law. A linear two-dimensional interpolation is used to evaluate the fields at the macroparticle positions and deflections are calculated assuming the fields are constant over one-quarter of the FODO cell. Finally, the motion of the ionized electrons is calculated between the bunch slices and the bunches, while the motion of the ions is calculated between bunches; in both cases, the motion is assumed to be nonrelativistic.

The simulation was written to study effects where the ions are strongly focused by the beam, so a number of simplifications were made. The primary omissions are as follows.

(i) The integration step is one-quarter of a FODO cell. This should not be a limitation since the beam distribution does not change much over this distance.

(ii) The fields are mapped onto a grid (typically 25×25) and the ion or electron macroparticles are created on this grid. Again, this is not an important limitation—we have verified that doubling the number of grid points does not significantly change the results.

(iii) The beam is assumed to be Gaussian when calculating the beam forces. This is valid provided the beam distribution is not strongly distorted.

(iv) Synchrotron motion of the beam particles and longitudinal motion of the ions are ignored. The longitudinal ion motion is insignificant over the passage of a single bunch train and the synchrotron motion can be neglected provided the growth rates are fast compared to the synchrotron frequency.

(v) Nonrelativistic motion is assumed for ions and atomic electrons. This is a reasonable assumption for the ions, whose typical velocity is of the order 3000–30 000 m/s. Strictly, in the case of electron bunches, the atomic electrons acquire velocities close to the speed of light, but they are lost so rapidly that they do not have any effect on the beam. In the case of positron bunches, where the atomic electrons are trapped inside a bunch, the nonrelativistic approximation is usually fulfilled. For instance, in the case of the SLC Positron Arc, the rms velocity of atomic electrons is about 4% c .

(vi) Ions and atomic electrons are generated at temper-

ature zero, i.e., with zero initial velocity. This is usually a good approximation for ions whose thermal velocity is about 300 m/s (and thus only 1–10 % of the velocity they have gained after the first bunch has passed), but it may not be a good approximation for the atomic electrons.

(vii) The simulation is based on a linear accelerator model. Accordingly, trapping of ions through the gap in a ring is not considered. For the high-current factory rings, this is a very good approximation. As an example, in the case of PEP-II, the residual CO ion density after the gap is only about 1% of the ion density before the gap.

(viii) In the simulations, the cross section for collisional ionization is held constant at a value of 2 Mb (corresponding to carbon monoxide and a beam energy of about 40 GeV). As in the analytical treatment, a second ionization and photoionization are not included.

(ix) Each simulation study includes a single species of ions (one particular value of the ion mass). If more than one species is present with a comparable abundance, the lightest molecule that is still stably trapped inside the bunch train will asymptotically determine the evolution of the instability since the corresponding rise time is the smallest. In such a case, the partial pressure for this particular molecule has to be used in the analytical estimate of the rise time Eq. (40).

The simulations described above have been performed for the PEP-II HER, the SLC Positron Arc, and the NLC Damping Ring. In the simulations of the SLC Positron Arc, the total number of macroparticles was 160 000 distributed over 80 slices in z , while in the case of PEP-II and the NLC Damping Ring, 20 000 macroparticles distributed over five slices were used per bunch. In the simulations, the transverse density of the generated ions becomes sharply peaked at the beam center. After the passage of a few electron bunches, the transverse density is quite different from a Gaussian distribution [15].

Figure 1 shows the vertical bunch centroid positions as a function of bunch number after a distance of 0, 750,

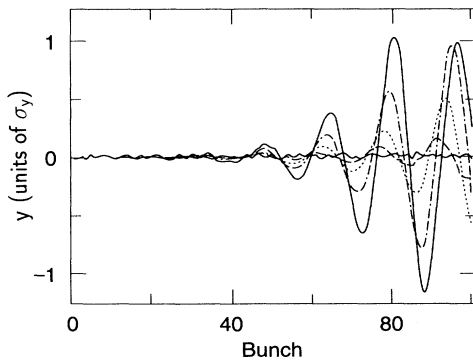


FIG. 1. Vertical beam centroid as a function of bunch number after a distance of 0 m (solid curve), 750 m (dashed curve), 1125 m (dotted curve), 1500 m (dash-dotted curve), and 1875 m (solid curve), respectively, for a train of 100 bunches, with an atomic mass of 28 (carbonmonoxide) and a pressure of 10^{-5} Torr in the arcs of the PEP-II HER.

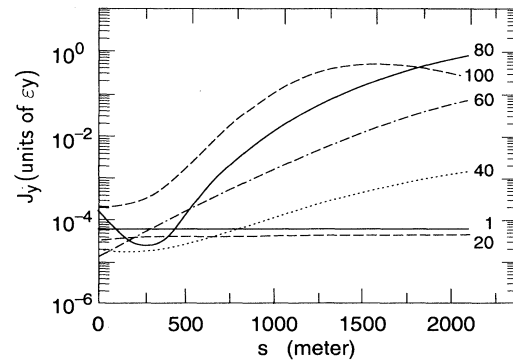


FIG. 2. Action of the vertical centroid as a function of distance for every 20th bunch of a train of 100 bunches in the PEP-II HER with a pressure of 10^{-5} Torr.

1125, 1500, and 1875 m, respectively, for a train of 100 bunches and a pressure of 10^{-5} Torr in the arcs of the PEP-II HER. Clearly visible is the instability at the tail of the train and the exponential growth of the vertical amplitude as a function of z (the bunch number). The amplitude growth slows down, or saturates, at about $1\sigma_y$ ($100 \mu\text{m}$) due to the nonlinearity of the beam-ion force and the detuning of ω_i at large amplitudes.

In Fig. 2 the action of the bunch centroid

$$J_y \equiv \frac{1}{2} \left[\frac{(1 + \alpha^2)}{\beta} \langle y \rangle^2 + 2\alpha \langle y \rangle \langle y' \rangle + \beta \langle y' \rangle^2 \right] \quad (46)$$

is depicted as a function of the distance in meters for every 20th bunch in the train. The initial amplitudes are due to the finite number of macroparticles and on average $\langle J_y \rangle = \epsilon_y / N_{\text{macro}}$. Notice that the initial growth from noise is not uniform, that it depends instead on the initial distribution of macroparticles, which will subsequently be discussed further. The growth rate of the trailing bunches for the real PEP-II HER extrapolated from this

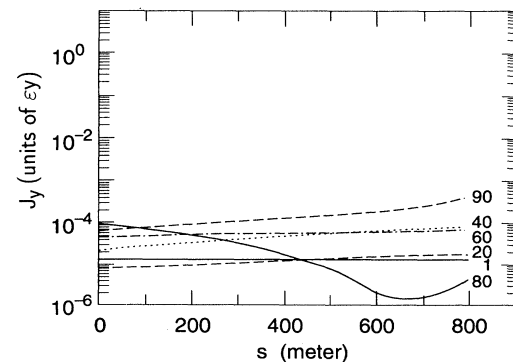


FIG. 3. Growth of the action of the vertical centroid for every 20th (plus last) of 90 bunches in the NLC DR for 10^{-8} Torr, an atomic mass of 28 (carbon monoxide), and 1.5×10^{10} particles per bunch over a distance of 800 m.

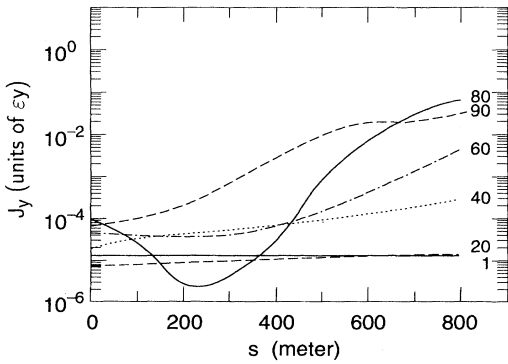


FIG. 4. Growth of the action of the vertical centroid for every 20th of 90 bunches in the NLC DR for 3×10^{-8} Torr, an atomic mass of 28 (carbon monoxide), and 1.5×10^{10} particles per bunch over a distance of 800 m.

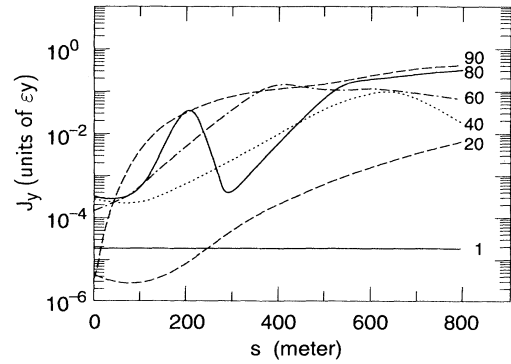


FIG. 6. Growth of the action of the vertical centroid for every 20th of 90 bunches in the NLC DR for the same conditions as Fig. 5 but using a different random seed for the macroparticle distribution.

scaled version is about $5 \mu\text{s}$; this is close to the estimate of $6 \mu\text{s}$ obtained from Eq. (40).

In Figs. 3–5 the action of every 20th bunch in the NLC Damping Ring is depicted for three different pressure values over a distance of 800 m. For bunch number 90, the action increases by a factor 9 after 800 m, 260 m, and 70 m at a pressure of 10^{-8} Torr, 3×10^{-8} Torr, and 10^{-7} Torr, respectively. This is in agreement with the expected scaling $s \propto 1/p$.

Figure 6 shows results obtained under the same conditions as the previous case (see Fig. 5), but using a different random seed for the initial beam macroparticle distribution. In this simulation, the rise time of bunch number 90 is roughly 9.8 ns, while in the previous case (Fig. 5), the rise time is 23 ns. The initial growth from noise is sensitive to the distributions of macroparticles and, because the growth saturates at roughly σ_y , we do not observe the full asymptotic behavior. We thus see large fluctuations in the simulation results. Typically,

the simulated growth times vary by less than an order of magnitude and, within this uncertainty, they agree with the analytic calculations. For example, the growth times in both Figs. 5 and 6 should be compared with the analytical estimate of 5 ns.

In Fig. 7 the conditions were the same as in Fig. 5 except for a smaller bunch charge, namely, 7×10^9 . The corresponding growth rate is smaller by about a factor 5, which is expected from the analytical result. Figure 8 shows results for an ion atomic mass of 44 (carbon dioxide), for which the rise time is about 25% larger than for carbon monoxide (see Fig. 5). This is again consistent with the analytical dependence. Finally, Figs. 9 and 10 show the position of the vertical beam and ion centroids along the bunch train after 0, 200, 400, and 600 m in the NLC Damping Ring when the pressure is 10^{-7} Torr; the data are from the same simulation as that in Fig. 5.

We have also performed simulations of the ion instability in the NLC prelinear accelerator and the NLC main linear accelerator and simulations of trapped electrons in the SLC Positron Arc, which transports positrons.

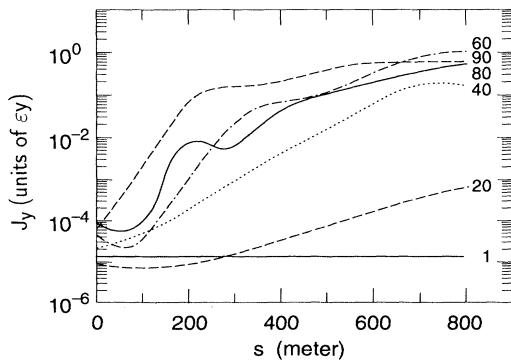


FIG. 5. Growth of the action of the vertical centroid for every 20th of 90 bunches in the NLC DR for 10^{-7} Torr, an atomic mass of 28 (carbon monoxide), and 1.5×10^{10} particles per bunch over a distance of 800 m.

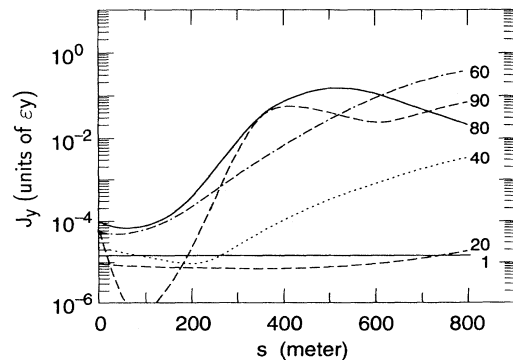


FIG. 7. Growth of the action of the vertical centroid in the NLC DR for 7×10^9 particles per bunch, an atomic mass of 28, and a pressure of 10^{-7} Torr.

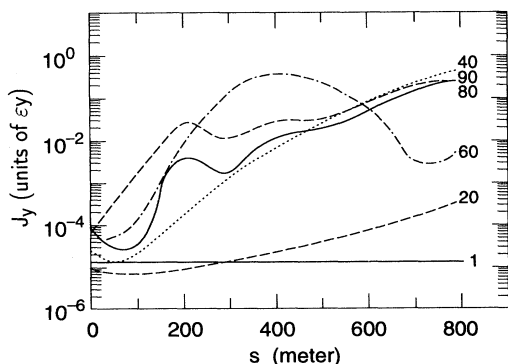


FIG. 8. Growth of the action of the vertical centroid in the NLC DR for carbon dioxide (atomic mass 44), 1.5×10^{10} particles per bunch, and a pressure of 10^{-7} Torr.

In these cases, as well as for those described above, we find that the simulation results are consistent with the analytical calculation. The growth rates found in the simulations agree with the analytical result to within a factor 2 or 3, which is comparable to the spread of values obtained for different random seeds. We should note that the simulations were typically performed at relatively high vacuum pressures to increase the growth rates and to reduce the simulation time. This introduces uncertainty when extrapolating to much lower vacuum pressures and growth rates, which, for example, is necessary in the PEP-II HER or NLC Damping Rings.

VI. RISE TIMES FOR EXISTING AND PLANNED ACCELERATORS

Table I shows basic accelerator parameters and the asymptotic growth times Eq. (40) and (41) for several accelerators proposed or under construction at SLAC and

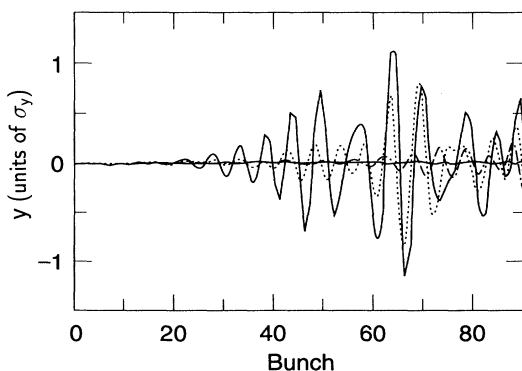


FIG. 9. Vertical beam centroid along the bunch train after 0 m (solid curve), 200 m (dashed curve), 400 m (dotted curve), and 600 m (solid curve) along the NLC DR at a pressure of 10^{-7} Torr; from the same simulation as Fig. 5.

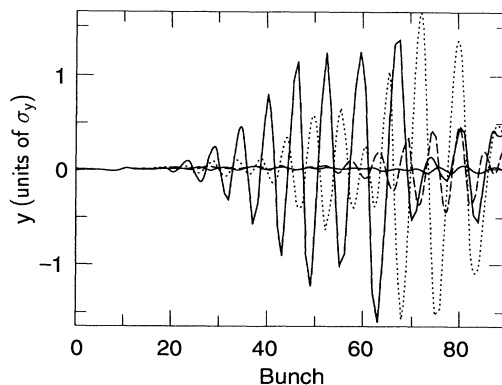


FIG. 10. Vertical ion centroid along the bunch train after 0 m (solid curve), 200 m (dashed curve), 400 m (dotted curve), and 600 m (solid curve) along the NLC DR at a pressure of 10^{-7} Torr (compare with Fig. 9).

KEK, namely, for the NLC Damping Rings and linear accelerators, the PEP-II HER, and the KEK Accelerator Test Facility (ATF) Damping Ring [16]. Due to its much higher vacuum pressure, the smallest rise time is expected for the ATF Damping Ring, which is planned to be in operation in 1996. The growth times listed are those for the trailing bunches ($z \approx z_0$). Values for the NLC systems vary between 40 ns and 1 μ s. Note again that τ_{asym} is not an e -folding time, but refers to an asymptotic amplitude growth of the form $y \propto \exp(\sqrt{t/\tau_{\text{asym}}})$. If the initial perturbation is purely due to Schottky noise, it takes about 200 times the quoted value of τ_{asym} before the bunches oscillate at an amplitude comparable to the beam size. Even with the additional factor 200, the growth times are still very short.

For comparison, Table II presents a similar set of numbers for existing accelerators, such as the SLC Positron Arc, the Advanced Light Source (ALS) at Lawrence Berkeley Laboratory (LBL), the European Synchrotron Radiation Facility (ESRF), the HERA electron ring at DESY, and the SLC Positron Damping Ring. For the SLC Positron Damping Ring, the expected rise time is much larger than the synchrotron period (10 μ s), in which case the instability cannot develop and the presented theory does not apply.

In Cornell Electron Storage Ring (CESR) the predicted rise time is not small compared with the radiation damping time (several milliseconds), while in the case of the HERA electron ring, the rise time is about a factor 1 or 2 larger than the damping time of the transverse multi-bunch feedback. In both cases, the ion-coupled instability might not be observed. Thus, among the existing machines considered, only the two light sources, ALS and ESRF, could show a significant ion-coupled instability. The growth time in the ALS is predicted to be about 2 μ s. Experience so far is unclear. Transverse instabilities are observed in the ALS, but these are not necessarily caused by ions. For the ESRF, the expected rise time is 50 μ s. This is about a factor 150 smaller than the ra-

TABLE I. Parameters and oscillation growth rates for some future accelerators.

Accelerator	NLC				PEP-II	ATF
	e^- DR	e^+ DR	Pre-linac	Main linac	HER	DR
ϵ_x^N (m)	3×10^{-6}	3×10^{-6}	3×10^{-6}	3×10^{-6}	5×10^{-4}	3×10^{-6}
ϵ_y^N (m)	3×10^{-8}	3×10^{-8}	3×10^{-8}	3×10^{-8}	2.5×10^{-5}	3×10^{-8}
n_b	90	90	90	90	1658	60
N_b	1.5×10^{10}	1.5×10^{10}	1.5×10^{10}	1.5×10^{10}	3×10^{10}	10^{10}
$\beta_{x,y}$ (m)	0.5,5	0.5,5	6	8	15	0.5,5
$\bar{\beta}_y$ (m)	2	2	6	8	15	2.5
σ_x (μm)	62	62	68	35	1,060	22
σ_y (μm)	4	4	7	3.5	169	7
z_0 (σ_z)	19 m	4 mm	19 m	19 m	1000 m	25 m
E (GeV)	2	2	2	10	9	1.54
p (Torr)	10^{-9}	10^{-9}	10^{-8}	10^{-8}	10^{-9}	6×10^{-8}
particle species	e^-	e^+	e^-	e^-	e^-	e^-
$\omega_{\text{ion}}/2\pi$ (MHz)	184	3.2×10^5	104	201	4	85
single or						
multibunch	multibunch	single	multibunch	multibunch	multibunch	multibunch
$\tau_{\text{asym}} (z \approx z_0)$	465 ns	122 μs	88 ns	46 ns	6 μs	29 ns

diation damping time and thus the beam-ion instability might also be observable here. However, there has been no evidence for ion-related effects or multibunch instabilities at the ESRF [17]. One possible explanation for the observed stability pertains to the distinct focusing optics: The ESRF uses a Chasman-Green lattice, in which the product of the horizontal and vertical β functions varies by more than a factor 100 around the ring. This causes a corresponding variation of the ion frequency by an order of magnitude. The decoherence of the ion motion due to this large frequency variation could effectively suppress the instability. Note that, by contrast, in a standard FODO lattice the product of the transverse beam sizes is nearly constant and thus this source of decoherence does not exist.

Because of the potential impact on B factory and NLC designs an experimental confirmation of analytical theory and computer simulations is highly desirable. An experiment to monitor and compare the emittance of electron

and positron beams as a function of the increased vacuum pressure in the SLC Arcs is therefore being proposed. At the current pressure of 10^{-5} Torr, the initial Fourier component at the ion frequency is enhanced by a modest 20% at the end of the arc. This effect is too small to be measurable. The “threshold” pressure for observable positron emittance growth is 3×10^{-4} to 10^{-3} Torr. Above the threshold, the positron emittance increases exponentially with an exponent proportional to $p^{1/2}$, while the electron emittance continues to increase quadratically due to an interplay of ions and dispersion as discussed in Ref. [18].

VII. POSSIBLE CURES

There are several possible ways to alleviate the described detrimental effect of ions or electrons. If the os-

TABLE II. Parameters and oscillation growth rates for some existing accelerators.

Accelerator	SLC arc	SLC e^+ DR	ALS	HERA e^-	CESR	ESRF
ϵ_x^N (m)	5×10^{-5}	3×10^{-5}	1.2×10^{-5}	2×10^{-3}	2.7×10^{-3}	7.5×10^{-5}
ϵ_y^N (m)	5×10^{-6}	3×10^{-6}	2×10^{-7}	1.1×10^{-4}	1.2×10^{-4}	7.5×10^{-6}
n_b	1	1	328	210	7	330
N_b	3.5×10^{10}	4×10^{10}	7×10^9	3.7×10^{10}	4.6×10^{11}	5×10^9
$\beta_{x,y}$ (m)	4	1,3	2.5,4	25	14,13	8,8
$\bar{\beta}_y$ (m)	4	3	4	25	13	8
σ_x (μm)	50	114	101	1000	2000	224
σ_y (μm)	15	62	17	230	400	70
z_0 (σ_z)	1 mm	5.9 mm	100 m	3024 m	335 m	140 m
E (GeV)	46	1.2	1.5	26	5	6
p (Torr)	10^{-5}	10^{-8}	10^{-9}	10^{-9}	5×10^{-9}	2×10^{-9}
particle species	e^+	e^+	e^-	e^-	e^-	e^-
$\omega_{\text{ion}}/2\pi$ (MHz)	4×10^5	5×10^4	25	0.8	0.6	8.3
Single or						
multibunch	single	single	multibunch	multibunch	multibunch	multibunch
$\tau_{\text{asym}} (z \approx z_0)$	1.1 μs	490 μs	2.4 μs	211 μs	3.9 ms	50 μs

cillation amplitude of the trailing bunches or positrons, respectively, saturates at about $1\sigma_y$ due to the nonlinear character of the coupling force (not included in the analytical treatment), a reduction of the vertical emittance by a factor 2 results in approximately the desired projected final emittance after filamentation [19]. It is not yet known if the beam will continue to blow up, although with a decreasing growth rate, after partial filamentation. A second possibility is to use an optical lattice in which the product of the horizontal and vertical β functions changes substantially as a function of position s so that ω_i varies significantly with time and no coherent oscillation can therefore develop. A third remedy consists in introducing additional gaps in the bunch train, large enough so that the ions are overfocused between the shorter trains [20]. As an example, additional ten bunch gaps in PEP-II increase the instability rise time from 5 μ s to 0.5 ms, which is inside the bandwidth of the feedback system. Finally, in linear accelerators, the trailing bunches might be realigned by use of fast kickers and feedforward.

VIII. SUMMARY AND OUTLOOK

The interaction of an electron bunch train or a single positron bunch with ions or ionization electrons causes a transverse instability. The signature of this instability is an exponential growth of the vertical amplitude, the exponent being directly proportional to the position along the bunch or bunch train and to the square root of time and inversely proportional to the 3/4 power of the beam sizes.

The expected rise time τ_{asym} of the instability is exceedingly short; it varies between 40 and 800 ns for the various NLC rings and linear accelerators, while it is estimated at 5 μ s for the PEP-II HER. This rise time is not an e -folding time, but the oscillation amplitude grows as $\exp(\sqrt{t/\tau_{\text{asym}}})$. As far as existing machines are concerned, the effect should be present in the ALS and possibly CESR, but observations so far are inconclu-

sive, partly due to technical problems and partly due to the similarity to transverse wake-field effects. An experiment to measure the emittance increase as a function of pressure in the SLC Arcs is being pursued to confirm the theory and the simulations described.

Several possible remedies have been suggested. The addition of ten short gaps in the bunch train might alleviate the problem for the PEP-II HER. It also may be possible to design lattices in which the ion frequency is strongly location dependent. Both of these options require further study. Finally, if the instability saturates at an amplitude of about 1σ , it is conceivable to design damping rings in which the equilibrium emittance is about half the desired emittance. Preliminary simulations indicate that the saturation is not complete and that further amplitude growth at a smaller rate is possible.

The analytical model described is a linearized approximation and does not include nonlinearities of the ion-beam force or the lattice. However, these nonlinearities are included in the simulations, which yield rise times for the parameter regimes compared that are in excellent agreement with the analytic model. It is not known at this time if and when the Landau damping due to the nonlinear ion-beam force becomes significant, and our model should be extended to include this effect [21]. A large number of other questions also remain to be answered. Among them are the saturation or filamentation due to detuning at large vertical amplitudes, the initial growth from noise, the effect of synchrotron motion on the growth rate, the rise time in the presence of different ion species, the possible damping due to the nonlinearity of the beam-beam interaction in circular colliders, and the study of coherent oscillation modes of higher order.

ACKNOWLEDGMENTS

We thank A. Chao, S. Heifets, and G. Stupakov for helpful discussions. This work was supported by Department of Energy Contract No. DE-AC03-76SF00515.

-
- [1] A. Chao, B. Richter, and Y. Yao, *Nucl. Instrum. Methods* **178**, 1 (1980).
 - [2] A. Chao, *Physics of Collective Beam Instabilities in High Energy Accelerators* (Wiley, New York, 1993).
 - [3] E. Keil and B. Zotter, CERN Report No. ISR-TH/71-58, 1971 (unpublished).
 - [4] R. Alves Pires *et al.*, *Proceedings of the 1989 IEEE Particle Accelerator Conference* (IEEE, New York, 1989), p. 800.
 - [5] E. Jones *et al.*, *Proceedings of the 1985 IEEE Particle Accelerator Conference* (IEEE, New York, 1985), p. 2218.
 - [6] A. Poncet, CERN Report No. CERN 90-04, 1990 (unpublished).
 - [7] A. Poncet, *Frontiers of Particle Beams: Intensity Limitations*, edited by Dienes *et al.*, Lecture Notes in Physics Vol. 400 (Springer-Verlag, Berlin, 1990).
 - [8] D. Sagan and A. Temnykh, *Nucl. Instrum. Methods Phys. Res. Sect. A* **344**, 459 (1994).
 - [9] G. Koshkarev and P. Zenkevich, *Particle Accelerators* **3**, 1 (1972).
 - [10] L. J. Laslett *et al.*, *Nucl. Instrum. Methods Phys. Res. Sect. A* **121**, 517 (1974).
 - [11] SLAC Report No. SLAC-418, 1993 (unpublished).
 - [12] The NLC is a future linear collider being designed at SLAC. Parameters for the damping rings and linear accelerators can be found in SLAC Report No. SLAC-436, 1994 (unpublished).
 - [13] The SLC arcs are 1.2-km achromatic transport lines that transport the electron and positron beams from the end of the SLAC linear accelerator to the final foci. Parameters can be found in *SLC Design Handbook* (Stanford Linear Accelerator Center, Stanford, 1986).

- [14] M. Bassetti and G. A. Erskine, CERN Report No. CERN-ISR-TH 80-06, 1980 (unpublished).
- [15] T. O. Raubenheimer and P. Chen, *Proceedings of the 1992 Linear Accelerator Conference* (Love Printing Services, Ontario, Canada, 1992), p. 630; P. F. Tavares, CERN Report No. CERN-PS-92-55, 1992 (unpublished).
- [16] J. Urakawa *et al.*, *Int. J. Phys. A (Proc. Suppl.)* **2B**, 124 (1993).
- [17] J. M. Filhol, *Proceedings of the Fourth European Particle Accelerator Conference* (World Scientific, Singapore, 1994), p. 8.
- [18] P. Emma, T. Raubenheimer, and F. Zimmermann, *Proceedings of the Fourth European Particle Accelerator Conference* (Ref. [17]), p. 1162.
- [19] K. Oide (private communication).
- [20] J. Seeman (private communication).
- [21] G. Stupakov, T. Raubenheimer, and F. Zimmermann, following paper, *Phys. Rev. E* **52**, 5499 (1995).